Loss and Thermal Noise in Plasmonic Waveguides

R.R.A.Syms*

Optical and Semiconductor Devices Group, EEE Dept., Imperial College London,

Exhibition Road, London SW7 2AZ, UK

*Corresponding Author

TEL +44-20745203

FAX +44-2076308

Email r.syms@imperial.ac.uk

L.Solymar

Optical and Semiconductor Devices Group, EEE Dept., Imperial College London,

Exhibition Road, London SW7 2AZ, UK

Abstract

Rytov's theory of thermally generated radiation is used to find the noise in two-dimensional passive guides based on an arbitrary distribution of lossy isotropic dielectric. To simplify calculations, the Maxwell curl equations are approximated using difference equations that also permit a transmission-line analogy and material losses are assumed to be low enough for modal losses to be estimated using perturbation theory. It is shown that an effective medium representation of each mode is valid for both loss and noise, and hence that a one-dimensional model can be used to estimate the best achievable noise factor when a given mode is used in a communications link. This model only requires knowledge of the real and imaginary parts of the modal dielectric constant. The former can be found by solving the lossless eigenvalue problem, while the latter can be estimated using perturbation theory. Because of their high loss, the theory is most relevant to plasmonic waveguides, and its application is demonstrated using single interface, slab and slot guide examples. The best noise performance is offered by the long-range plasmon supported by the slab guide.

KEYWORDS: Dielectric waveguide, Plasmonic waveguide, Loss, Noise, Fluctuation-dissipation theorem

PACS numbers 41.20.-q Applied classical electromagnetism
73.20.Mf Surface plasmons
07.50.Hp Noise, electrical circuits

1. Introduction

The development of long-distance optical communications was a major technological success of the 21st century. Necessary conditions were the availability of waveguides with low dispersion and low loss. Alternative structures based on metals and dielectrics – plasmonic guides – are being proposed for on-chip communication [1-3]. However, collision damping in metals causes high attenuation. Consequently, there has been intensive interest in arrangements with low loss. The earliest example is the 'long-range' plasmon supported by a thin metal slab, which achieves its effect by extending the modal field outside the metal [4-6]. Narrow metal strips, which loosen the confinement further, are now being investigated [7-9], as are wires [10-12], slots [13-16] and grooves [17-19]. Amplification using a dye has also been proposed to compensate for losses [20, 21].

Communication systems also suffer from noise. In fibre optics, propagation loss is so low that the focus is on amplified spontaneous emission in amplifiers [22-24] and Johnson and shot noise in the receiver [25]. Noise theories have already been developed for active plasmonics [26, 27] and their implications are being explored [28]. However, because losses are much higher in plasmonics, thermal noise may be more significant. Noise was first observed experimentally in resistors by Johnson [29], and its relation to loss explained in classical and quantum-mechanical terms by Nyquist [30] and Callen and Welton [31]. The general relation is known as the fluctuation-dissipation (FD) theorem. In the 1950s, Rytov developed a model for thermal radiation by adding sources derived from the FD theorem to the Maxwell curl equations [32]. However, Rytov only explored

simple waveguide problems, the effect of walls or inclusions in hollow waveguides [33]. Emission from such guides forms the basis of microwave noise standards [34].

Rytov's methods are hard to apply to general geometries. Spurred by the development of metamaterials, for which an equivalent circuit model is realistic, we have developed a transmission line approach to one-dimensional (1D) thermal noise, which involves replacement of differentials with discrete equivalents [35]. The problem of integrating the effect of noise sources is then replaced with summation. Analytic proofs – that noise is linked to effective medium properties – may then be arrived at easily. Emission and related metrics such as the noise factor may be computed directly, and additional effects such as noise carried by internal lattice waves may also be incorporated [36].

Here, we adapt the method to more general 2D guides. Once again, we use difference equations that allow a transmission-line analogy. To simplify calculations, losses are assumed to be low, so perturbation theory can be used. Because most dielectric guides have low loss and TEM-like modes, there are few literature discussions of loss or polarization effects. An exception is the difference between TE and TM mode gain in semiconductor lasers [37, 38]. However, losses are much higher in plasmonics, and polarization is crucial. Here both polarizations are considered together. The aim is to prove that modal noise is directly linked to modal effective medium properties, and hence that noise can be computed directly in a 1D calculation. If this can be done, thermal noise may easily be incorporated into transmission line models of plasmonics [39], or network models of amplification [40]. The wave equation is discussed in Section 2, the waveguide

equation in Section 3, and perturbation expressions for loss in Section 4. The link between modal noise and loss is derived in Section 5, and a method of calculating the noise factor in Section 6. The performance of three different plasmonic waveguides is compared in Section 7, and conclusions are drawn in Section 8.

2. The discrete model and the wave equation

We first develop a transmission line representation for the geometry of Figure 1a, namely a z-propagating waveguide described by a general dielectric constant variation $\varepsilon(x)$ in the transverse direction. The Maxwell curl equations reduce to:

$$\begin{aligned} \text{TE:}\quad & \partial H_x/\partial z - \partial H_z/\partial x = +j\omega\varepsilon E_y \\ & \partial E_y/\partial z = +j\omega\mu_0 H_x \\ & \partial E_y/\partial x = -j\omega\mu_0 H_z \end{aligned} \qquad \begin{aligned} \text{TM:}\quad & \partial E_x/\partial z - \partial E_z/\partial x = -j\omega\mu_0 H_y \\ & \partial H_y/\partial z = -j\omega\varepsilon E_x \\ & \partial H_y/\partial x = +j\omega\varepsilon E_z \end{aligned} \tag{1}$$

Here E_x, E_y and E_z and H_x, H_y and H_z are x-, y- and z-components of the time-independent electric and magnetic fields at angular frequency ω, and μ_0 and ε are the permeability of free space and the more general permittivity. We represent both polarizations using the 2D transmission-line model of Figure 1b. Here the lattice is of side a, the fields are represented by a nodal voltage $V_{m,n}$ and line currents $I_{Xm,n}$ and $I_{Zm,n}$, and material parameters are represented using per-unit length inductance and capacitance L_{Pm} and C_{Pm} that vary only with the transverse index m. The circuit equations are:

$$\begin{aligned} (I_{Xm,n} - I_{Xm-1,n})/a + (I_{Zm,n} - I_{Zm,n-1})/a &= -j\omega C_{Pm} V_{m,n} \\ (V_{m+1,n} - V_{m,n})/a &= -j\omega L_{Pm} I_{Xm,n} \\ (V_{m,n+1} - V_{m,n})/a &= -j\omega L_{Pm} I_{Zm,n} \end{aligned} \tag{2}$$

Comparison with (1) shows that the field and circuit quantities must map together as

shown in Table I. The transmission line must then be different for each polarization. For TE (Figure 2a), the series inductors represent magnetic properties and the shunt capacitors dielectric properties. For TM (Figure 2b), it is the other way around. This conclusion is counter-intuitive, but the circuit analogy is best considered as an aid to calculation rather than a physical model. The effect of noise in the dielectric may then conveniently be represented by shunt current sources $J_{m,n}$ (for TE) and series voltage sources $U_{Xm,n}$ and $U_{Zm,n}$ (for TM). Their values will be discussed later.

	C_{Pm}	L_{Pm}	$V_{m,n}$	$I_{Xm,n}$	$I_{Zm,n}$
TE	$\varepsilon(x)$	μ_0	$E_y(x, z)$	$H_z(x, z)$	$-H_x(x, z)$
TM	μ_0	$\varepsilon(x)$	$H_y(x, z)$	$-E_z(x, z)$	$E_x(x, z)$

Table I. Mapping of electromagnetic field and transmission line quantities for TE and TM modes.

When single modes are propagating, it would be desirable to reduce the circuits to 1D equivalents as shown in Figures 3a (for TE) and 3b (for TM). Here ε_ν is the effective dielectric constant of the ν^{th} mode, and $J_{\nu n}$ are current sources (for TE) and $U_{\nu n}$ are voltage sources (for TM) that describe the dielectric noise coupled into the ν^{th} mode. Also shown are source and load components, which will also be discussed later. Generally there will be a set of 1D effective medium models, one for each mode.

To derive the wave equation for the discrete model it is helpful to define column vectors $\underline{X}_n$ with $\underline{X}_n(m) = X_{m,n}$ that represent all values of a field quantity for a given n, and diagonal matrices $\underline{Y}$ with $\underline{Y}(m, m) = Y_m$ that represent material parameters. It is also useful to define first-order backward and forward difference operators Δ_{Bn} and Δ_{Fn} for the

n-direction such that $\underline{\Delta}_{Bn}\underline{X}_n = (\underline{X}_n - \underline{X}_{n-1})/a$ and $\underline{\Delta}_{Fn}\underline{X}_n = (\underline{X}_{n+1} - \underline{X}_n)/a$. Clearly, $\underline{\Delta}_{Fn}\underline{\Delta}_{Bn}\underline{X}_n = (\underline{X}_{n+1} - 2\underline{X}_n + \underline{X}_{n-1})/a^2$. We may refer to this quantity as $\underline{\Delta}_n^2\underline{X}_n$, where $\underline{\Delta}_n^2$ is a second-order difference operator. Similar matrix operators $\underline{\Delta}_{Bm}$ and $\underline{\Delta}_{Fm}$ can be defined for the m-direction; these are banded matrices such that $\underline{\Delta}_{Bm}(m, m) = 1/a$, $\underline{\Delta}_{Bm}(m, m-1) = -1/a$, $\underline{\Delta}_{Fm}(m, m) = -1/a$ and $\underline{\Delta}_{Fm}(m, m+1) = 1/a$. Again, $\underline{\Delta}_{Bm}\underline{\Delta}_{Fm} = \underline{\Delta}_{Fm}\underline{\Delta}_{Bm} = \underline{\Delta}_m^2$, where $\underline{\Delta}_m^2$ is a banded matrix with $\underline{\Delta}_m^2(m, m-1) = 1/a^2$, $\underline{\Delta}_m^2(m, m) = -2/a^2$ and $\underline{\Delta}_m^2(m, m+1) = 1/a^2$. With this notation, (2) becomes:

$$\underline{\Delta}_{Bm}\underline{I}_{Xn} + \underline{\Delta}_{Bn}\underline{I}_{Zn} = -j\omega\underline{C}_P\underline{V}_n$$

$$\underline{\Delta}_{Fm}\underline{V}_n = -j\omega\underline{L}_P\underline{I}_{Xn}$$

$$\underline{\Delta}_{Fn}\underline{V}_n = -j\omega\underline{L}_P\underline{I}_{Zn} \tag{3}$$

This approach is clearly directly analogous to the well-established transmission-line matrix method [41, 42], and related to the method of lines [43], which only uses discretization in one direction. Elimination of the currents $\underline{I}_{Xn}$ and $\underline{I}_{Zn}$ then yields the wave equation:

$$\underline{\Delta}_{Bm}\underline{L}_P^{-1}\underline{\Delta}_{Fm}\underline{V}_n + \underline{L}_P^{-1}\underline{\Delta}_n^2\underline{V}_n + \omega^2\underline{C}_P\underline{V}_n = 0 \tag{4}$$

The analysis can be used for TE or TM, merely by assuming the correct values of L_P and C_P from Table I. In terms of a diagonal relative dielectric constant matrix $\underline{\varepsilon}_r$, we obtain:

Discrete Continuous

TE: $(\underline{\Delta}_m^2 + \Delta_n^2 + k_0^2\underline{\varepsilon}_r)\underline{V}_n = 0$ $\quad\quad$ $\partial^2E_y/\partial x^2 + \partial^2E_y/\partial z^2 + k_0^2\varepsilon_rE_y = 0$

TM: $(\underline{\Delta}_{Bm}\,\underline{\varepsilon}_r^{-1}\,\underline{\Delta}_{Fm} + \underline{\varepsilon}_r^{-1}\Delta_n^2 + k_0^2)\underline{V}_n = 0$ $\quad$ $\partial/\partial x\{1/\varepsilon_r\,\partial H_y/\partial x\} + (1/\varepsilon_r)\partial^2H_y/\partial z^2 + k_0^2H_y = 0$

(5)

where $k_0^2 = \omega^2\mu_0\varepsilon_0$. Here we also show the continuous equations [44], which correspond.

3. The waveguide equation and modal solutions

Assumption of a modal solution $\underline{V}_n = \underline{v} \exp(-j\beta na)$ where $\underline{v}$ is a fixed vector and β is the propagation constant then yields the waveguide equation:

$$\underline{\Delta}_{Bm}\underline{L}_P^{-1}\underline{\Delta}_{Fm}\,\underline{v} + \omega^2\underline{C}_P\underline{v} + (2/a^2)\{\cos(\beta a) - 1\}\underline{L}_P^{-1}\underline{v} = 0 \qquad (6)$$

This equation can now be recast as a generalized eigenvalue problem, namely:

$$\underline{A}\underline{v} = \lambda\underline{B}\underline{v} \qquad (7)$$

where $\underline{A} = \underline{\Delta}_{Bm}\underline{L}_P^{-1}\underline{\Delta}_{Fm} + \omega^2\underline{C}_P$, $\underline{B} = \underline{L}_P^{-1}$ and $\lambda = (2/a^2)\{1 - \cos(\beta a)\}$. Equation 7 replaces the problem of solving Maxwell's equations with that of finding the eigenvectors of a matrix. There is no need for boundary matching, and arbitrary permittivity variations may be incorporated, including steps. It has set of eigensolutions, which should be compared with the modes $E_y = E_\mu(x)\exp(-j\beta_\mu z)$ (for TE) and $H_y = H_\mu(x)\exp(-j\beta_\mu z)$ (for TM) in the continuous model. Clearly the eigenvectors $\underline{v}_\mu$ correspond to the transverse fields E_μ or H_μ. Since $\lambda \approx \beta^2$ if βa is small, the eigenvalues λ_μ correspond to the squares of the propagation constants β_μ^2. Writing $\beta_\mu^2 = k_0^2\varepsilon_{r\mu}$, where $\varepsilon_{r\mu}$ is a relative dielectric constant for the mode, we obtain the waveguide equations:

	Discrete	Continuous
TE:	$(\underline{\Delta}_m^2 + k_0^2\underline{\varepsilon}_r)\underline{v}_\mu = k_0^2\varepsilon_{r\mu}\underline{v}_\mu$	$d^2E_\mu/dx^2 + k_0^2\varepsilon_r E_\mu = k_0^2\varepsilon_{r\mu}E_\mu$

TM: $(\underline{\Delta}_{Bm}\underline{\varepsilon}_r^{-1}\underline{\Delta}_{Fm} + k_0^2)\underline{v}_\mu = k_0^2\varepsilon_{r\mu}\,\underline{\varepsilon}_r^{-1}\underline{v}_\mu$ $\quad d/dx\,\{1/\varepsilon_r\, dH_\mu/dx\} + k_0^2 H_\mu = k_0^2\varepsilon_{r\mu}H_\mu/\varepsilon_r$

(8)

Here we also show the continuous equations [44], which again correspond.

When $\underline{A}$ and $\underline{B}$ are symmetric and loss-less, different eigenvectors $\underline{v}_\nu$ and $\underline{v}_\mu$ must satisfy the orthogonality relation $\underline{v}_\nu{}^{*T}\underline{B}\underline{v}_\mu = 0$. When $\nu \neq \mu$, we then obtain

	Discrete	Continuous
TE:	$\underline{v}_\nu{}^{*T}\underline{v}_\mu = 0$	$\int_{-\infty}^{\infty} E_\nu{}^* E_\mu\, dx = 0$
TM:	$\underline{v}_\nu{}^{*T}\underline{\varepsilon}_r^{-1}\underline{v}_\mu = 0$	$\int_{-\infty}^{\infty} H_\nu{}^*(1/\varepsilon_r)H_\mu\, dx = 0$

(9)

For dielectric guides, transverse fields are normalised so that the inner products above yield delta functions $\delta_{\nu\mu}$, simplifying subsequent calculations. However, because ε_r is negative in a lossless metal, TM inner products must be negative for modes that have their field concentrated in metal. Because these modes cannot then be normalised to unity, we will work with un-normalised fields.

The time-averaged power is $P = 1/2\ \mathrm{Re}(\underline{I}_{Zn}{}^{*T}\underline{V}_n)$. If only the μ^{th} mode is propagating, so that $\underline{V}_n = a_\mu\underline{v}_\mu \exp(-j\beta_\mu na)$, we obtain the following expressions for power:

	Discrete	Continuous
TE:	$P_\mu = (\beta_\mu/2\omega\mu_0)a_\mu a_\mu{}^*(\underline{v}_\mu{}^{*T}\underline{v}_\mu)$	$P_\mu = (\beta_\mu/2\omega\mu_0)a_\mu a_\mu{}^*(\int_{-\infty}^{\infty} E_\mu{}^* E_\mu\, dx)$

TM: $P_\mu = (\beta_\mu/2\omega\varepsilon_0)a_\mu a_\mu^*(\underline{v}_\mu^{*T}\underline{\varepsilon}_r^{-1}\underline{v}_\mu)$ $P_\mu = (\beta_\mu/2\omega\varepsilon_0)a_\mu a_\mu^*\{\int_{-\infty}^{\infty} H_\mu^*(1/\varepsilon_r)H_\mu\, dx\}$

(10)

Once again, we have compared the discrete equations with their continuous counterparts.

The eigensolutions will include both guided and radiation modes. However, because the matrix must in practice be finite in size, the calculation window must also be restricted. With minor modifications (to ensure continuity of diagonal elements of the matrix $\underline{\Delta}_{Bm}\underline{L}_P^{-1}\underline{\Delta}_{Fm}$) the effect is to introduce perfect conductor boundaries. Guided modes may be modeled realistically, by choosing the range of m so that their transverse fields are sufficiently confined inside the window. However, the spectrum of radiation modes will be discretized, and general calculations will show spurious effects caused by boundary reflection. These may be reduced, by introducing absorbing boundary elements [43].

4. Loss

The effect of introducing loss to an otherwise loss-less guide can be estimated using perturbation theory. A standard result of the generalized eigenvalue problem is that the first-order change $\Delta\lambda_\mu$ in λ_μ caused by changes $\underline{\Delta A}$ and $\underline{\Delta B}$ to $\underline{A}$ and $\underline{B}$ is:

$$\Delta\lambda_\mu = \{\underline{v}_\mu{}^{*T}\underline{\Delta A}\underline{v}_\mu - \lambda_\mu\underline{v}_\mu{}^{*T}\underline{\Delta B}\underline{v}_\mu\}/(\underline{v}_\mu{}^{*T}\underline{B}\underline{v}_\mu) \tag{11}$$

In terms of changes $\underline{\Delta L_P}$ and $\underline{\Delta C_P}$ to $\underline{L_P}$ and $\underline{C_P}$, we can write $\underline{\Delta A} = -\underline{\Delta}_{Bm}\underline{\Delta L_P}\underline{L_P}^{-2}\underline{\Delta}_{Fm} + \omega^2\underline{\Delta C_P}$ and $\underline{\Delta B} = -\underline{\Delta L_P}\underline{L_P}^{-2}$. Here, we will be interested in perturbations caused by the introduction of loss to a previously loss-less system. If we write complex dielectric constants and eigenvalues as $\varepsilon = \varepsilon' - j\varepsilon''$ and as $\lambda_\mu = \lambda_\mu' - j\lambda_\mu''$, Equation 11 will allow determination of the value of λ_μ'' caused by ε''. Such results are again usefully expressed in terms of relative dielectric constants, as:

Discrete

TE: $\varepsilon_{r\mu}'' = (\underline{v}_\mu{}^{*T}\underline{\varepsilon}_r''\underline{v}_\mu)/(\underline{v}_\mu{}^{*T}\underline{v}_\mu)$

TM: $\varepsilon_{r\mu}'' = \{\varepsilon_{r\mu}'\underline{v}_\mu{}^{*T}\underline{\varepsilon}_r''\underline{\varepsilon}_r'^{-2}\underline{v}_\mu - (1/k_0{}^2)\underline{v}_\mu{}^{*T}\underline{\Delta}_{Bm}\underline{\varepsilon}_r''\underline{\varepsilon}_r'^{-2}\underline{\Delta}_{Fm}\underline{v}_\mu\}/(\underline{v}_\mu{}^{*T}\underline{\varepsilon}_r'^{-1}\underline{v}_\mu)$

Continuous

TE: $\varepsilon_{r\mu}'' = \{\int_{-\infty}^{\infty} E_\mu{}^*\varepsilon_r''E_\mu\,dx\}/\{\int_{-\infty}^{\infty} E_\mu{}^*E_\mu\,dx\}$

TM:

$$\varepsilon_{r\mu}'' = \{\int_{-\infty}^{\infty} \varepsilon_{r\mu}'H_\mu{}^*(\varepsilon_\mu''/\varepsilon_r'^2)H_\mu - (1/k_0{}^2)H_\mu{}^*d/dx[(\varepsilon_r''/\varepsilon_r'^2)dH_\mu/dx]\,dx\}/\{\int_{-\infty}^{\infty} H_\mu{}^*\varepsilon_r^{-1}H_\mu\,dx\} \tag{12}$$

5. Noise

If the effect of modal noise may be represented by sources $J_{m,n}$ (for TE) and $U_{Xm,n}$ and $U_{Zm,n}$ (for TM), the loss terms above should define the noise. To prove this, it is necessary to find the noise coupled into the μ^{th} mode from the sources in the 2D model, and show that the value corresponds with the 1D model. To do so, we follow Rytov's procedure.

TE modes

The calculation is simplest for TE modes (Fig. 2a). We first note that it is only necessary to show that the results match along one line, say n = 0, and that the noise sources are independent. We therefore start by considering a single source at (0, 0). Its effects are readily included in Equations (2) or (3). The TE wave equation (8) will be valid except on n = 0, where there must be an additional excitation term on the RHS:

$$(\underline{\Delta}_m^2 + \Delta_n^2 + k_0^2\underline{\varepsilon}_r)\underline{V}_0 = -j(\omega\mu_0/a)J_{0,0}\underline{\delta}(0) \qquad (13)$$

Here $\underline{\delta}(0)$ is a vector containing a single unit element at m = 0. Clearly, the source will radiate in all directions, and excite all the modes in some proportion. However, symmetry implies that the overall solution must have the form:

$$\underline{V}_n = \sum_\mu a_\mu \underline{V}_\mu \exp(-j\beta_\mu na) \text{ for } n \geq 0$$

$$\underline{V}_n = \sum_\mu a_\mu \underline{V}_\mu \exp(+j\beta_\mu na) \text{ for } n \leq 0$$

(14)

Here, the coefficients a_μ are unknown modal amplitudes. These solutions satisfy the TE wave equation automatically for $n \neq 0$. Exactly on $n = 0$, however, we get:

$$\sum_\mu a_\mu\{\underline{\Delta}_m^2 + 2[\exp(-j\beta_\mu a) - 1]/a^2 + k_0^2\underline{\varepsilon}_r\}\underline{v}_\mu = -j(\omega\mu_0/a)J_{0,0}\underline{\delta}(0)$$

(15)

Eliminating terms using the TE waveguide equation, and assuming that $\beta_\mu a$ is small, this result simplifies to $\sum_\mu a_\mu\beta_\mu\underline{v}_\mu = (\omega\mu_0/2)J_{0,0}\underline{\delta}(0)$. Pre-multiplying both sides by $\underline{v}_\nu{}^{*T}$ and making use of TE mode orthogonality we may extract the mode amplitude a_ν as

$$a_\nu = (\omega\mu_0/2\beta_\nu)v_{\nu 0}{}^*J_{0,0}/(\underline{v}_\nu{}^{*T}\underline{v}_\nu)$$

(16)

From the above we may then obtain $a_\nu a_\nu{}^* = (\omega\mu_0/\beta_\nu)^2 v_{\nu 0}{}^*(J_{0,0}J_{0,0}{}^*/4)v_{\nu 0}/(\underline{v}_\nu{}^{*T}\underline{v}_\nu)^2$ and an analogous expression for a source at a different point (m, 0). Since the sources are independent, we may sum these terms incoherently to obtain the total effect as:

$$a_\nu a_\nu{}^* = (\omega\mu_0/\beta_\nu)^2\{\sum_m v_{\nu m}{}^*(J_{m,0}J_{m,0}{}^*/4)v_{\nu m}\}/(\underline{v}_\nu{}^{*T}\underline{v}_\nu)^2$$

(17)

The values of the thermal sources $J_{m,0}$ are defined by the FD theorem, which implies that an admittance Y will give rise to a current J whose RMS value in a frequency interval df is $JJ^* = 4W\mathrm{Re}(Y)df$. Here $W = (hf/2)\coth(hf/K\Theta)$ is the mean energy at absolute temperature Θ of an oscillator of natural frequency $\omega = 2\pi f$, and h and K are Planck's and Boltzmann's constants. Here, $Y = j\omega\varepsilon_0(\varepsilon_{rm}' - j\varepsilon_{rm}'')a$, so $J_{m,0}J_{m,0}{}^* = 4W\omega\varepsilon_0\varepsilon_{rm}''adf$. Hence

we may write:

$$a_\nu a_\nu^* = (\omega\mu_0/\beta_\nu)^2(W\omega\varepsilon_0 adf)\{{}_m\Sigma\, v_{\nu m}^*\varepsilon_{rm}''v_{\nu m}\}/(\underline{v}_\nu^{*T}\underline{v}_\nu)^2 \qquad (18)$$

Now, the term ${}_m\Sigma\, v_{\nu m}^*\varepsilon_{rm}''v_{\nu m}$ will be recognised as $\underline{v}_\nu^{*T}\underline{\varepsilon}_r''\underline{v}_\nu$. Comparison with Equation (12) then shows that $a_\nu a_\nu^* = (\omega\mu_0/\beta_\nu)^2 W\omega\varepsilon_0\varepsilon_{r\nu}'' adf / (\underline{v}_\nu^{*T}\underline{v}_\nu)$. For RMS values - which require multiplication of expressions in (10) by two - the noise power coupled into the ν^{th} mode at n = 0 is then:

$$P_{\nu TE2} = (\omega\mu_0/\beta_\nu)W\omega\varepsilon_0\varepsilon_{r\nu}''adf \qquad (19)$$

Considering now the 1D TE model of Fig. 3a, it is simple to show that $\beta_\nu^2 = k_0^2\varepsilon_{r\nu}$, so the 2D and 1D TE models are equivalent as far as propagation is concerned. It is also simple to show that the effect of a single current source $J_{\nu 0}$ at n = 0 is to launch a pair of counter-propagating voltage waves whose forward amplitude is $A_\nu = (\omega\mu_0/\beta_\nu)J_{\nu 0}/2$. For RMS values, the power carried by this wave is $P_{\nu TE1} = (\omega\mu_0/\beta_\nu)J_{\nu 0}J_{\nu 0}^*/4$. Now, from the FD theorem, the sources in the 1D model satisfy $J_{\nu 0}J_{\nu 0}^* = 4W\omega\varepsilon_0\varepsilon_{r\nu}''adf$. Consequently, $P_{\nu TE1}$ is exactly as given in (19), and the 2D and 1D TE mode systems are also equivalent as far as noise power is concerned.

TM Modes

We now repeat the process for the TM model of Fig. 3b. The calculation is more difficult,

since there are two sets of sources that generate more complicated effects. However, we again need only show that the 2D and 1D results match on n = 0. We begin by considering the voltage sources $U_{Zm,n}$, and to start with allow a source only at (0, 0). Generally the TM wave equation in (8) will be valid. However, there must now be an excitation term on the RHS at m = 0 for two lines, n = 0 and n = 1. Here, we get:

$$(\underline{\Delta}_{Bm}\underline{\varepsilon}_r^{-1}\underline{\Delta}_{Fm} + \underline{\varepsilon}_r^{-1}\Delta_n^2 + k_0^2)\underline{V}_0 = (1/\varepsilon_{r0}a^2)U_{Z0,0}\underline{\delta}(0)$$

$$(\underline{\Delta}_{Bm}\underline{\varepsilon}_r^{-1}\underline{\Delta}_{Fm} + \underline{\varepsilon}_r^{-1}\Delta_n^2 + k_0^2)\underline{V}_1 = -(1/\varepsilon_{r0}a^2)U_{Z0,0}\underline{\delta}(0) \qquad (20)$$

The source will again excite waves in all directions on a 2D plane. This time, the excitation suggests an anti-symmetric response, of the form:

$$\underline{V}_n = {}_\mu\Sigma\ -a_\mu\underline{v}_\mu \exp(+j\beta_\mu na) \text{ for } n \le 0$$

$$\underline{V}_n = {}_\mu\Sigma\ a_\mu\underline{v}_\mu \exp\{-j\beta_\mu(n-1)a\} \text{ for } n \ge 1 \qquad (21)$$

Substitution into either of Equations (20) gives the same result, so only one need be considered. Following a similar procedure (eliminating terms using the TM waveguide equation, assuming small $\beta_\mu a$, pre-multiplying both sides by $\underline{v}_\nu{}^{*T}$ and making use of TM mode orthogonality), the amplitude a_ν can be found. The effects of all the sources $U_{Zm,0}$ may then be found as:

$$a_\nu a_\nu{}^* = {}_m\Sigma\ v_{\nu m}{}^*(U_{Zm,0}U_{Zm,0}{}^*/4)(1/\varepsilon_{rm}{}^2)v_{\nu m}/(\underline{v}_\nu{}^{*T}\underline{\varepsilon}_r{}^{t-1}\underline{v}_\nu)^2 \qquad (22)$$

Once again, the FD theorem specifies the sources, as $U_{Zm,0}U_{Zm,0}^* = 4W\omega\varepsilon_0\varepsilon_{rm}''adf$.

Substituting into (22) then yields:

$$a_v a_v^* = (W\omega\varepsilon_0 adf)\underline{v}_v{}^{*T}\underline{\varepsilon}_r''\underline{\varepsilon}_r^{-2}\underline{v}_v/(\underline{v}_v{}^{*T}\underline{\varepsilon}_r'^{-1}\underline{v}_v)^2 \tag{23}$$

We must now repeat the process for the sources $U_{Xm,n}$, again starting with a single one at (0, 0). Once there must now be additional excitation terms in the wave equation at n = 0. This time, equations at m = 0 and m = 1 are affected, and:

$$(\underline{\Delta}_{Bm}\underline{\varepsilon}_r^{-1}\underline{\Delta}_{Fm} + \underline{\varepsilon}_r^{-1}\Delta_n^2 + k_0^2)\underline{V}_0 = -(1/\varepsilon_{r0}a)U_{X0,0}\underline{\Delta}_{Fm}\underline{\delta}(0) \tag{24}$$

This time the response must be symmetric, so we assume:

$$\underline{V}_n = \sum_\mu a_\mu \underline{v}_\mu \exp(-j\beta_\mu na) \text{ for } n \geq 0$$

$$\underline{V}_n = \sum_\mu a_\mu \underline{v}_\mu \exp(+j\beta_\mu na) \text{ for } n \leq 0 \tag{25}$$

Following the same procedure, the effect of all the noise sources may be obtained as:

$$a_v a_v^* = -(1/\beta_v^2)(W\omega\varepsilon_0 adf)\,\underline{v}_v{}^{*T}\underline{\Delta}_{Bm}\underline{\varepsilon}_r''\underline{\varepsilon}_r^{-2}\underline{\Delta}_{Fm}\underline{v}_v/(\underline{v}_v{}^{*T}\underline{\varepsilon}_r'^{-1}\underline{v}_v)^2 \tag{26}$$

The combined effect of both sets of noise sources is then:

$$a_v a_v^* = (W\omega\varepsilon_0 adf)\{\underline{v}_v{}^{*T}\underline{\varepsilon}_r''\underline{\varepsilon}_r^{-2}\underline{v}_v - (1/\beta_v^2)\underline{v}_v{}^{*T}\underline{\Delta}_{Bm}\underline{\varepsilon}_r''\underline{\varepsilon}_r^{-2}\underline{\Delta}_{Fm}\underline{v}_v\}/(\underline{v}_v{}^{*T}\underline{\varepsilon}_r'^{-1}\underline{v}_v)^2$$

(27)

Comparison with the result of perturbation theory (12) shows that the two separate loss terms are directly linked to the two noise terms, and that $a_\nu a_\nu^* = (1/\varepsilon_{r\nu}')W\omega\varepsilon_0\varepsilon_{r\nu}''adf/(\underline{v}_\nu^{*T}\underline{\varepsilon}_r'^{-1}\underline{v}_\nu)$. For RMS values, the power coupled into the ν^{th} mode at n = 0 is:

$$P_{\nu TM2} = (\beta_\nu/\omega\varepsilon_\nu')W\omega\varepsilon_0\varepsilon_{r\nu}''adf$$

(28)

For the 1D model of Fig. 3b, $\beta_\nu^2 = k_0^2\varepsilon_{r\nu}$ as before, so the 2D and 1D TM models are again equivalent as far as propagation is concerned. The effect of a single voltage source $U_{\nu 0}$ at n = 0 is to launch counter-propagating waves with equal and opposite amplitudes. For the forward-going wave, the amplitude is $A_\nu = U_{\nu 0}/2$ and the power is $P_{\nu TM1} = (\beta_\nu/\omega\varepsilon_\nu')U_{\nu 0}U_{\nu 0}^*/4$. From the FD theorem, $U_{\nu 0}U_{\nu 0}^* = 4W\omega\varepsilon_0\varepsilon_{r\nu}''adf$. Consequently, $P_{\nu TM1}$ is then as given in (28), and the 2D and 1D TM models are equivalent for noise. Thus, the reduction from Figures 2 to 3 is entirely robust. Furthermore, since $\beta_\nu^2 = \omega^2\mu_0\varepsilon_\nu'$, $P_{\nu TE1} = P_{\nu TM1}$ so the noise power is independent of polarization, and simply depends on the loss. In fact, both can be expressed as $P_\nu = Z_\nu W\omega\varepsilon_\nu''adf$, where $Z_\nu = \sqrt{(\mu_0/\varepsilon_\nu)}$ is the characteristic impedance of the ν^{th} mode.

6. Noise factor

We now use the 1D model to estimate the performance of a waveguide link. We assume the source emits a signal power P_S and noise P_{SN}, so that the input signal-to-noise ratio (SNR) is P_S/P_{SN}. We also assume the link has transmittance T and emits a forward noise power P_N, so that the output SNR is $P_S T/(P_{SN}T + P_N)$. Hence the noise factor F is:

$$F = 1 + P_N/P_{SN}T \tag{29}$$

F may therefore be found by adding a noisy source to a noisy circuit and calculating the powers $P_{SN}T$ and P_N reaching the load. For TE modes, the complete circuit is as shown in Figure 3a. Here, the source and load have real impedance Z_S. Assuming (as here) that the standard noise temperature is Θ, the effective input noise temperature Θ_n may then be related to the noise factor as $\Theta_n = \Theta(F - 1) = \Theta P_N/P_{SN}T$.

We now assume that the source is thermal, and at the same temperature Θ. Consequently, the RMS value of the source noise voltage U_S is $U_S U_S^* = 4WZ_S df$. If in addition the source and load are free space, we can put $Z_S = \sqrt{(\mu_0/\varepsilon_0)}$. $P_{SN}T$ may be found by calculating the load power with only the source noise U_S present. Similarly, P_N may be found by summing the load powers from each of the waveguide noise sources J_{vn}. The noise figure NF can then be found as $10 \log_{10}(F)$. If the bandwidth is wide, all contributions to noise must be integrated in frequency. Simplifications arise if the

bandwidth is narrow, when df may be used simply as a multiplier. In this case, the oscillator energy W in P_N and P_{SN} must cancel in F.

For TM modes, the complete circuit is as shown in Figure 3b. Here the source and load have characteristic impedance $Y_S = 1/Z_S$, and the source noise is generated by a current source J_S, whose RMS value is $J_S J_S^* = 4WY_S df$. With these assumptions, the nodal equations for TE and TM are the same if currents are exchanged for voltages. Consequently, all powers must also be the same, as must be the noise factor. TE and TM modes can therefore both be modelled using Figure 3a; this circuit is analogous to one derived in [35] for lossy slabs.

Since the discontinuities at the input and output are purely changes in impedance, the circuit models the system in Figure 3c. Here lossless optics couple a beam from free space into the guide, and then back into free space. The optics must act as a mode filter, to avoid excitation of modes other than the ν^{th} at the input, and to collect power only from this mode at the output. If it does not, less power will be coupled into the ν^{th} mode (reducing P_{SN}) and thermal noise will be detected from other modes (increasing P_N). Because both effects increase F, (29) is a lower bound.

7. Plasmonic waveguides

We now present examples from plasmonics. For simplicity we assume that all dielectric is air ($\varepsilon_{rd} = 1$), and that all metal can be described using the Drude model:

$$\varepsilon_{rm} = 1 - \omega_p^2/(\omega^2 - j\omega\omega_\tau) \tag{30}$$

Here ω_p and ω_τ are the plasma and collision damping frequencies. We assume that the metal is silver (with $\omega_p = 12.2 \times 10^{15}$ rad/s and $\omega_\tau = 0.09 \times 10^{15}$ rad/s). For angular frequencies ω significantly above ω_τ we may use the approximation $\varepsilon_{rm} = \varepsilon_{rm}' - j\varepsilon_{rm}''$, where $\varepsilon_{rm}' = 1 - \omega_p^2/\omega^2$ and $\varepsilon_{rm}'' = \omega_p^2\omega_\tau/\omega^3$.

Lossless plasmonic guides

We consider three different plasmonic guides: the single-interface (Figure 4a), slab (Figure 4b) and slot (Figure 4c). In each case, the lossless solutions are well known [13].

The single interface supports a solitary guided mode, whose magnetic field is:

$$H_y(x) = H_0\exp(-\gamma_{mP}x) \text{ for } x \geq 0$$
$$H_y(x) = H_0\exp(\gamma_{dP}x) \text{ for } x \leq 0 \tag{31}$$

Here $\gamma_{mP} = k_0\sqrt{(\varepsilon_{rP}' - \varepsilon_{rm}')}$ and $\gamma_{dP} = k_0\sqrt{(\varepsilon_{rP}' - \varepsilon_{rd}')}$ and ε_{rP}' is the relative dielectric constant of the mode. The eigenvalue equation can be found by matching tangential electric fields, as:

$$\gamma_{mP}/\gamma_{dP} + \varepsilon_{rm}'/\varepsilon_{rd} = 0 \tag{32}$$

Solving and re-arranging, ε_{rP}' can be found analytically as:

$$\varepsilon_{rP}' = \varepsilon_{rm}'\varepsilon_{rd}/(\varepsilon_{rd} + \varepsilon_{rm}') \tag{33}$$

The propagation constant is $\beta_P = k_0\sqrt{(\varepsilon_{rP}')}$. In fact, ε_{rP}' will only be positive if $\varepsilon_{rm}' < -\varepsilon_{rd}$, so cutoff will occur here at $\omega_p/\sqrt{2}$.

The slab supports two modes, with symmetric and anti-symmetric magnetic fields. For the mode with symmetric H_y (the long-range plasmon or ω^+ mode), the variations are:

$$H_y = H_0\exp\{\gamma_{dS}(x + h/2)\} \text{ for } x \le -h/2$$

$$H_y = H_0\cosh(\gamma_{mS}x)/\cosh(\gamma_{mS}h/2) \text{ for } |x| \le h/2$$

$$H_y = H_0\exp\{-\gamma_{dS}(x - h/2)\} \text{ for } x \ge h/2 \tag{34}$$

Here $\gamma_{mS} = k_0\sqrt{(\varepsilon_{rS}' - \varepsilon_{rm}')}$ and $\gamma_{dS} = k_0\sqrt{(\varepsilon_{rS}' - \varepsilon_{rd}')}$ and ε_{rS}' is the relative dielectric constant of the mode. The eigenvalue equation is:

$$(\gamma_{mS}/\gamma_{dS})\tanh(\gamma_{mS}h/2) + \varepsilon_{rm}'/\varepsilon_{rd} = 0$$

(35)

Similarly, for the mode with anti-symmetric H_y (the ω^- mode), the variations are:

$$H_y = -H_0\exp\{\gamma_{dA}(x + h/2)\} \text{ for } x \le -h/2$$

$$H_y = H_0\sinh(\gamma_{mA}x)/\sinh(\gamma_{mA}h/2) \text{ for } |x| \le h/2$$

$$H_y = H_0\exp\{-\gamma_{dA}(x - h/2)\} \text{ for } x \ge h/2$$

(36)

Here $\gamma_{mA} = k_0\sqrt{(\varepsilon_{rA}' - \varepsilon_{rm}')}$, $\gamma_{dA} = k_0\sqrt{(\varepsilon_{rA}' - \varepsilon_{rd}')}$ and ε_{rA}' is the relative modal dielectric constant. The eigenvalue equation is:

$$(\gamma_{mA}/\gamma_{dA})\coth(\gamma_{mA}h/2) + \varepsilon_{rm}'/\varepsilon_{rd} = 0$$

(37)

The eigenvalue equations must be solved numerically for ε_{rS}' and ε_{rA}'. Once this has been done, the propagation constants $\beta_S = k_0\sqrt{(\varepsilon_{rS}')}$ and $\beta_A = k_0\sqrt{(\varepsilon_{rA}')}$ may be found.

Depending on the thickness of the dielectric layer and the polarization, the slot structure can support a more extensive spectrum of guided modes. Here we focus on the two plasmonic modes with symmetric and anti-symmetric H_y, whose fields and dispersion equations can be found by exchanging the metal and dielectric terms in Equations 34-37. Once again, the dispersion equation can be solved numerically.

Perturbation expressions for loss

Calculation of the modal loss simply requires evaluation of (12). For general guides, a numerical calculation can be carried out using the matrix expressions. However, since the guided modes considered here are available analytically, direct integration may be used. For the single interface and the slab, we obtain:

$$\varepsilon_{rP}'' = \varepsilon_{rm}'' \{(2\varepsilon_{rP}' - \varepsilon_{rm}')/\varepsilon_{rm}'^2\}/(1/\varepsilon_{rm}' - \varepsilon_{rm}'/\varepsilon_{rd}^2)$$

$$\varepsilon_{rS}'' = \varepsilon_{rm}'' \{f_{S1}\varepsilon_{rS}'/\gamma_m\varepsilon_{rm}'^2 + f_{S2}(\varepsilon_{rS}' - \varepsilon_{rm}')/\gamma_m\varepsilon_{rm}'^2\}/(1/\gamma_{dS}\varepsilon_{rd} + f_{S1}/\gamma_m\varepsilon_{rm}')$$

$$\varepsilon_{rA}'' = \varepsilon_{rm}'' \{f_{A1}\varepsilon_{rA}'/\gamma_m\varepsilon_{rm}'^2 + f_{A2}(\varepsilon_{rA}' - \varepsilon_{rm}')/\gamma_m\varepsilon_{rm}'^2\}/(1/\gamma_{dA}\varepsilon_{rd} + f_{A1}/\gamma_m\varepsilon_{rm}') \quad (38)$$

Here:

$$f_{S1} = \{t_{mS} + (\gamma_{mS}h/2)(1 - t_{mS}^2)\} \text{ and } f_{S2} = \{t_{mS} - (\gamma_{mS}h/2)(1 - t_{mS}^2)\}$$
$$f_{A1} = \{c_{mA} + (\gamma_{mA}h/2)(1 - c_{mA}^2)\} \text{ and } f_{A2} = \{c_{mA} - (\gamma_{mA}h/2)(1 - c_{mA}^2)\} \quad (39)$$

where $t_{mS} = \tanh(\gamma_{mS}h/2)$ and $c_{mA} = \coth(\gamma_{mA}h/2)$. Similarly, for the slot, we get:

$$\varepsilon_{rS}'' = \varepsilon_{rm}'' \{\varepsilon_{rS}'/\gamma_m\varepsilon_{rm}'^2 + (\varepsilon_{rS}' - \varepsilon_{rm}')/\gamma_m\varepsilon_{rm}'^2\}/(1/\gamma_m\varepsilon_{rm}' + f_S/\gamma_{dS}\varepsilon_{rd})$$

$$\varepsilon_{rA}'' = \varepsilon_{rm}'' \{\varepsilon_{rA}'/\gamma_m\varepsilon_{rm}'^2 + (\varepsilon_{rA}' - \varepsilon_{rm}')/\gamma_m\varepsilon_{rm}'^2\}/(1/\gamma_m\varepsilon_{rm}' + f_A/\gamma_{dA}\varepsilon_{rd}) \quad (40)$$

Here:

$$f_S = \{t_{dS} + (\gamma_{dS}h/2)(1 - t_{dS}^2)\}$$

$$f_A = \{c_{dA} + (\gamma_{dA}h/2)(1 - c_{dA}^2)\}$$

(41)

where $t_{dS} = \tanh(\gamma_{dS}h/2)$ and $c_{dA} = \coth(\gamma_{dA}h/2)$. Finally we note that some modes can become backward waves. In this case, power flow is reversed; the simplest method of including this eventuality is to work with absolute values of ε_{rv}''.

Numerical results - modal fields and dispersion

We first briefly demonstrate that the matrix method generates realistic results. For simplicity, we consider only the single-interface guide, at the particular frequency for which $\varepsilon_{rm} = -10$. Figure 5a shows the variation of $|H_y|$ for the guided mode and some low-order radiation modes of the lossless structure. The modes are normalised so that $\underline{v}_v{}^{*T}\underline{\varepsilon}_r{}^{-1}\underline{v}_v = \pm 1$, so that modes concentrated in the metal (which has a large value of $|\varepsilon_r|$) appear large.

The field of the plasmon falls off exponentially on either side of the interface. Since the calculation window has been chosen so that the field has decayed sufficiently at the edges of the calculation window, the results are indistinguishable from analytic theory. The radiation modes are standing waves, with zeros forced by the perfect magnetic conductor (PMC) boundaries. Modes with ε_{rv} just less than ε_{rd} have their energy predominantly in the dielectric, while modes with ε_{rv} just below ε_{rm} are concentrated in the metal. These results are also indistinguishable from analytic theory, assuming the presence of PMC boundaries.

Figure 5b compares the predictions of the matrix method (points) and analytic theory (full line) for the plasmon dispersion characteristic. Detailed investigations show departures from full agreement at low frequency (when the characteristic approaches the light line) if the calculation window is too small, and at high frequency (when the characteristic tends to $\omega = \omega_p/\sqrt{2}$) if the size of the matrix is too small. However, with a suitable matrix, the two agree well over the whole frequency range. We have investigated other cases involving TE and TM modes; the matrix method generally gives good results.

Numerical results - noise

We now use the matrix method to demonstrate the excitation of radiation by noise sources. Figure 6 shows the variation of $|H_y|$ for the field generated in the lossy structure by the two noise sources at the point (0, 0), just at the edge of the metal. Figure 6a shows the results obtained with a standard matrix $\underline{A}$. Here, power coupled into radiation in the dielectric is reflected from the edge of the calculation window to create a confusing standing wave pattern. Figure 6b shows the results when the matrix elements are modified to provide a 10-layer broadband absorber at either edge of the window. Absorbing boundaries clearly eliminate most of the boundary reflection, and it is now clear that the effect of the excitation is mainly to launch the plasmon itself, together with a lobe of radiation in the dielectric. Radiation into the metal is quickly damped, because radiation modes concentrated here have negative relative dielectric constants even in the lossless case.

Numerical results - waveguide performance

We now compare the performance of the three different plasmonic guides. Figure 7a compares the dispersion characteristics for plasmons on single interfaces, slabs and slots. Two sets of data are shown, for h = 200 nm (LH) and h = 20 nm (RH). When h is large, all modes are forward waves and their dispersion characteristics are similar for most of the frequency range (except the slot plasmon with anti-symmetric H_y, whose dispersion characteristic is band-pass rather than low-pass). This behaviour can be understood by comparing the three dispersion equations; when $\gamma_m h/2$ is large, $\tanh(\gamma_m h/2)$ and $\coth(\gamma_m h/2)$ tend to unity, and the equations tend together. However, the equation for slot guides has $\gamma_d h/2$ instead of $\gamma_m h/2$, so there is a difference at low frequency. When h is small, there are much larger differences. The dispersion characteristics of the slab and slot modes with symmetric and anti-symmetric H_y are split about that of the single-interface plasmon, and the anti-symmetric slab and symmetric slot modes are backward for some or all of the frequency range.

Figure 7b shows the frequency variations of ε_r'' over the same range. When h is large, the modes again have similar attenuation. This behaviour can again be understood by considering the values of f_{S1}, f_{S2}, f_{A1} and f_{A2} in (39) and f_S and f_A in (41). All tend to unity when $\tanh(\gamma_m h/2)$ tends to unity, so that the perturbation expressions for loss tend together. However, when h is small, there are again differences. The slot modes typically have high loss, and are therefore of less interest. However, the attenuation characteristics

of the slab modes are split about that of the single-interface plasmon, and the slab mode with symmetric H_y has low value of ε_m'' over a wide spectral range. Common explanations are the extension of the evanescent field into the dielectric and the presence of a zero in the dominant electric field component (which is antisymmetric) in the metal.

Figure 7c shows the frequency variation of the noise figure, calculated assuming a 10 μm long guide sub-divided into 200 sections. Even over this short distance, the noise figures of most modes are greater than 10 dB over much of the available bandwidth, for both values of h, and the asymmetric mode of the slot waveguide is entirely out of scale for h = 20 nm. Any such modes might be considered unusable for practical on-chip communication. However, when h is small, the slab mode with symmetric H_y has a noise figure of only a few dB up until $\omega/\omega_p = 0.5$, as might be expected from its loss variation. This mode therefore offers the best loss and noise performance.

8. Conclusions

Using a discrete form of Rytov's theory for thermally generated radiation, we have proved that the noise properties of all two-dimensional guides based on distributions of isotropic dielectric can be determined from their modal effective medium properties. The noise sources distributed over the cross-section of a lossy waveguide scatter exactly the correct amount of power into each mode to make this equivalence possible. It is likely that similar proofs may be obtained using continuous theory, and for three-dimensional guides.

We have also presented a simple transmission line model that allows direct calculation of emission. All that is required are the real and imaginary parts of the modal dielectric constant. The former can be found by solving the lossless eigenvalue equation, and the latter may then be estimated using perturbation theory. This model allows the noise performance of different guides to be compared, and is especially relevant to plasmonics (where collision damping causes high loss). Not unnaturally, the best noise performance is obtained from the plasmonic guide with the lowest propagation loss. The model effectively assumes perfect source-waveguide and waveguide-load coupling, and hence estimates the best possible performance. However, more complicated models could be developed to include coupling into and out of multiple modes. To describe excitation, these would require a lossless splitting network between the source and a set of parallel transmission lines, one for each mode being considered. To describe detection, a similar lossless splitting network would be needed between the transmission lines and the load.

It is likely that equivalent circuit models may also be developed for non-thermal sources, and also for waveguides with distributed amplification. An important question then will be the relative magnitudes of amplified spontaneous emission from the gain medium and amplified thermal noise from the metal. Finally, we note that the method is simple enough to incorporate into general simulation tools that use circuit-based or discrete approximations.

9. References

1. Maier S.A., Brongersma M.L., Kik P.G., Meltzer S., Requicha A.A.G., Atwater H.A. "Plasmonics - a route to nanoscale optical devices" Adv. Mater. 13, 1501-1505 (2001)
2. Barnes W.L., Dereux A., Ebbesen T.W. "Surface plasmon subwavelength optics" Nature 424, 824-830 (2003)
3. Krenn J.R., Ditlbacher H., Schider G., Hohenau A., Leitner A., Aussenegg F.R. "Surface plasmon micro- and nano-optics" J. Microsc. 209, 167-172 (2009)
4. Oliner A.A., Tamir A. "Backward waves on isotropic plasma slabs" J. Appl. Phys. 33, 231-233 (1962)
5. Sarid D. "Long-range surface plasma waves on very thin metal films" Phys. Rev. Lett. 47, 1927-1930 (1981)
6. Craig A.E., Olson G.A., Sarid D. "Experimental observation of the long-range surface-plasmon polariton" Opt. Lett. 8, 380-382 (1983)
7. Berini P. "Plasmon-polariton modes guided by a metal film of finite width" Opt. Lett. 24, 1011-1013 (1999)
8. Charbonneau R., Berini P., Berolo E., Lisicka-Shrzek E. "Experimental observation of plasmon-polariton waves supported by a thin metal film of finite width" Opt. Lett. 25, 844-846 (2000)
9. Weeber J.-C., Krenn J.R., Dereux A., Lamprecht B., Lacroute Y., Goudonnet J.P. "Near-field observation of surface plasmon polariton propagation in thin metal stripes" Phys. Rev. B 64, 045411 (2001)

10. Pfeiffer C.A., Economou E.N. "Surface polaritons in a circularly cylindrical interface: surface plasmons" Phys. Rev. B 10, 3038-3051 (1974)
11. Takahara J., Yamagishi S., Taki H., Morimoto A., Kobayashi A. "Guiding of a one-dimensional optical beam with nanometer diameter" Opt. Lett. 22, 475-477 (1997)
12. Dickson R.M., Lyon L.A. "Unidirectional plasmon propagation in metallic nanowires" J. Phys. Chem. B 104, 6095-6098 (2000)
13. Economou E.N. "Surface plasmons in thin films" Phys. Rev. 182, 539-554 (1969)
14. Tanaka K., Tanaka M. "Simulations of nanometric optical circuits based on surface plasmon polariton gap waveguide" Appl. Phys. Lett. 82, 1158-1160 (2003)
15. Almeida V.R., Xu Q., Barrios C.A., Lipson M. "Guiding and confining light in void nanostructures" Optics Letts. 29, 1209-1211 (2004)
16. Veronis G., Fan S. "Guided subwavelength plasmonic mode supported by a slot in a thin metal film" Opt. Lett. 30, 3359-3361 (2005)
17. Novikov I.V., Maradudin A.A. "Channel polaritons" Phys. Rev. B 66, 035403 (2002)
18. Pile D.F., Gramotnev D.K. "Channel plasmon-polariton in a triangular groove on a metal surface" Opt. Lett. 29, 1069-1071 (2004)
19. Bozhevolnyi S.I., Volkov V.S., Devaux E., Ebbesen T.W. "Channel plasmon-polariton guiding by subwavelength metal grooves" Phys. Rev. Lett. 95, 046802 (2005)
20. De Leon I., Berini P. "Theory of surface plasmon-polariton amplification in planar structures incorporating dipolar gain media" Phys. Rev. B. 161401(R) (2008)
21. De Leon I., Berini P. "Amplification of long-range surface plasmons by a dipolar

gain medium" Nature Photonics 4, 382-387 (2010)

22. Mukai T., Yamamoto Y., Limura T. "Semiconductor laser pre-amplifier and linear repeater systems" IEEE Trans. Micr. Theory Tech. MTT-30, 1548-1558 (1982)
23. Desurvire E. "Amplification of spontaneous emission in erbium-doped single-mode fibers" J. Lightwave Tech. 7, 835-845 (1989)
24. Olsson N.A. "Lightwave systems with optical amplifiers" J. Lightwave Tech. 7, 1071-1082 (1989)
25. Yariv A. "Optical electronics" 3rd Edn., Holt, Reinhart and Winston, New York (1985)
26. De Leon I., Berini P. "Theory of noise in high-gain surface plasmon-polariton amplifiers incorporating dipolar gain media" Optics Express 19, 20506-20517 (2011)
27. De Leon I., Berini P. "Measuring gain and noise in active surface plasmon-polariton waveguides" Rev. Sci. Inst. 82, 033107 (2011)
28. Thylen L., Holmstren P., Bratkovsky A., Li J., Wang S.-Y. "Limits on integration as determined by power dissipation and signal-to-noise ratio in loss-compensated photonic integrated circuits based on metal/quantum dot materials" IEEE J. Quant. Elect. 46, 518-524 (2010)
29. Johnson J.B. "Thermal agitation of electricity in conductors" Phys. Rev. 32, 97-109 (1928)
30. Nyquist H. "Thermal agitation of electric charge in conductors" Phys. Rev. 32, 110-113 (1928)
31. Callen H.B., Welton T.A. "Irreversibility and generalized noise" Phys. Rev. 83, 34-40 (1951)

32. Rytov S.M. “Theory of electrical fluctuations and thermal radiation” Academy of Sciences, Moscow (1953) (translated as AFCRC-TR-59-162)
33. Rytov S.M. “On thermal radiation in waveguides” J. Exp. Theor. Phys. 27.5, 571-578 (1954)
34. Stelzried C. “Microwave thermal noise standards” IEEE Trans. Micr. Theory Tech. MTT-16, 646-655 (1968)
35. Syms R.R.A., Sydoruk O., Solymar L. “Transmission line model of noisy electromagnetic media” IEEE Trans. Micr. Theory Tech. 61, 14-22 (2013)
36. Syms R.R., Sydoruk O., Solymar L. “Noise in 1D metamaterials supporting magneto-inductive lattice waves” Phys. Rev. B. 87, 155155 (2013)
37. Visser T.D., Demeulenaere B., Haes J., Lenstra D., Baets R., Blok H. “Confinement and modal gain in dielectric waveguides” J. Lightwave Tech. 14, 885-887 (1996)
38. Haes J., Demeulenaere B., Baets R., Lenstra D., Visser T.D., Blok H. “Difference between TE and TM modal gain in amplifying waveguides: analysis and assessment of two perturbation approaches” Opt. Quant. Elect. 29, 263-273 (1997)
39. Kocabas S.E., Veronics G., Miller D.A.B., Fan S. “Transmission line and equivalent circuit models for plasmonic waveguide components” IEEE J. Sel. Top. Quant. Elect. 14, 1452-1472, (2008)
40. Berglind E., Gillner L. “Optical quantum noise treated with classical electrical network theory” IEEE J. Quant. Elect. 30, 846-853 (1994)
41. Johns R.P., Beurle R.L. “Numerical solution of 2-dimensional scattering problems using a transmission-line matrix” Proc. IEE 118, 1203-1208 (1971)
42. Johns P.B. “Application of the transmission-line-matrix method to homogeneous

waveguides of arbitrary cross-section" Proc. IEE 119, 1087-1091 (1972)

43. Pregla R. "The method of lines" in "*Analysis of Electromagnetic fields and waves*", John Wiley and Sons, Chichester (2008)

44. Marcuse D. "*Light transmission optics*" Van Nostrand Reinhold, New York (1972)

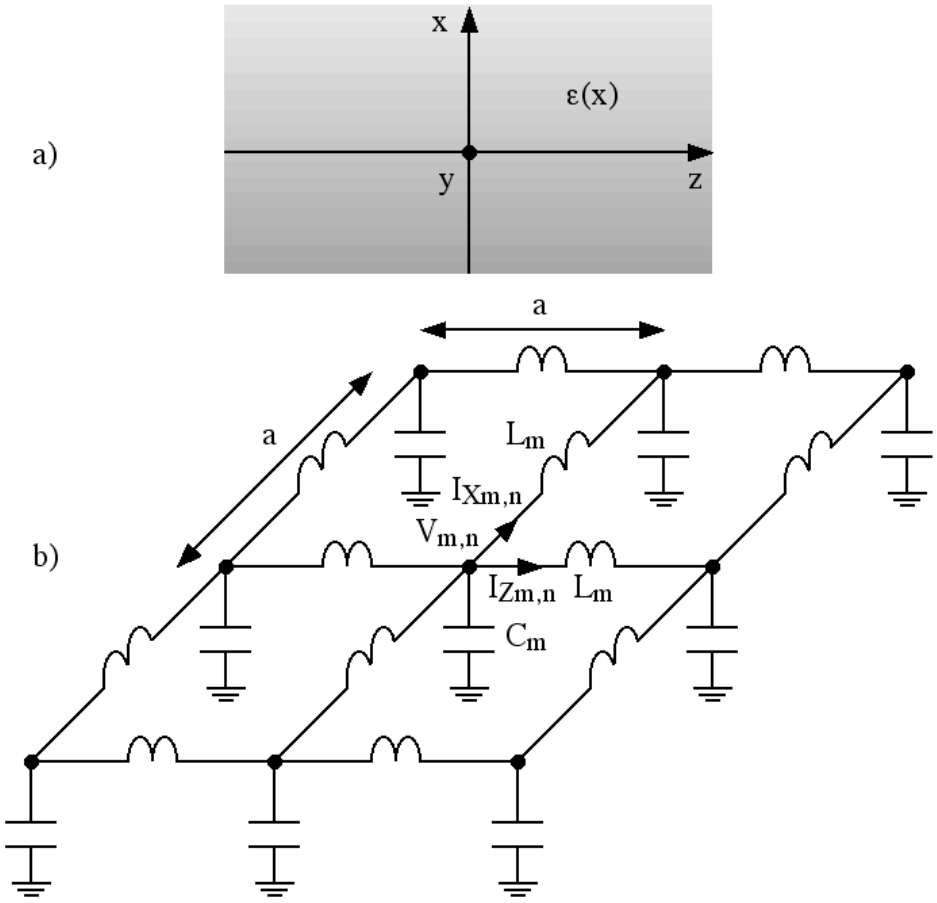

Figure 1. Graded 2D waveguide in a) continuous and b) transmission-line models.

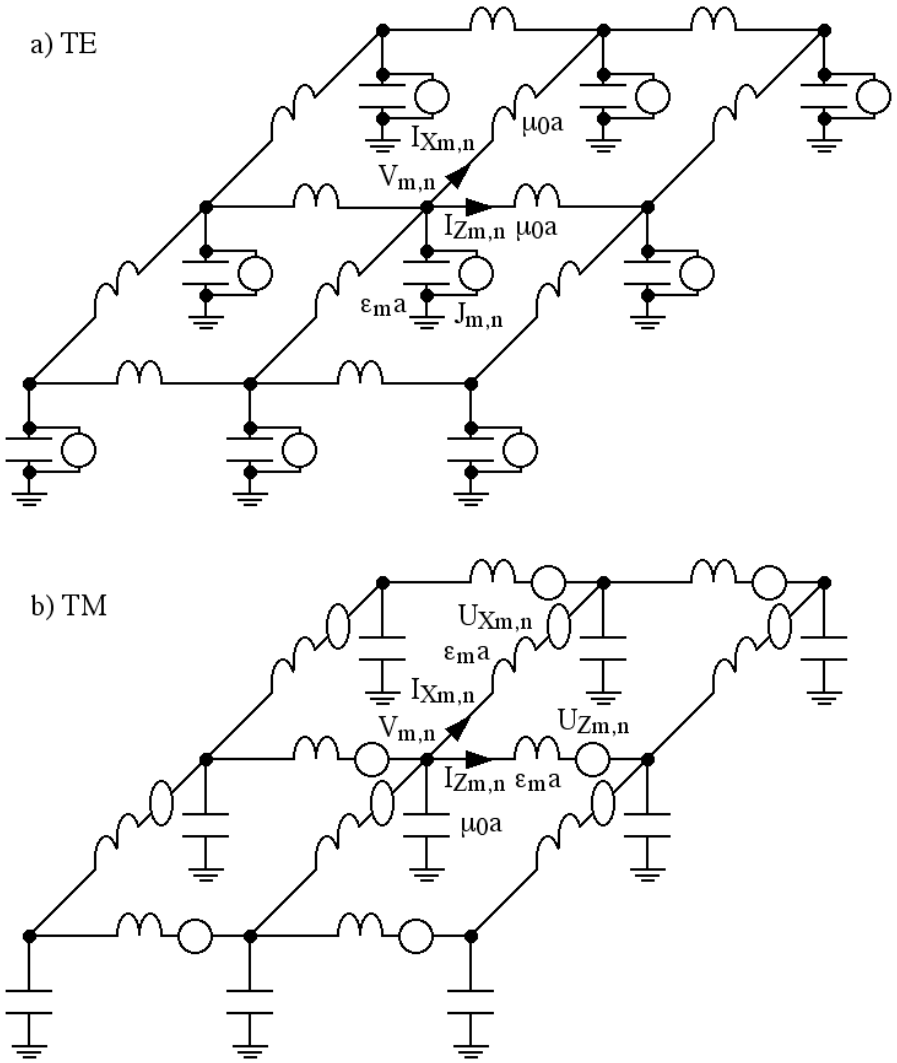

Figure 2. 2D transmission line models for a) TE and b) TM, with noise sources.

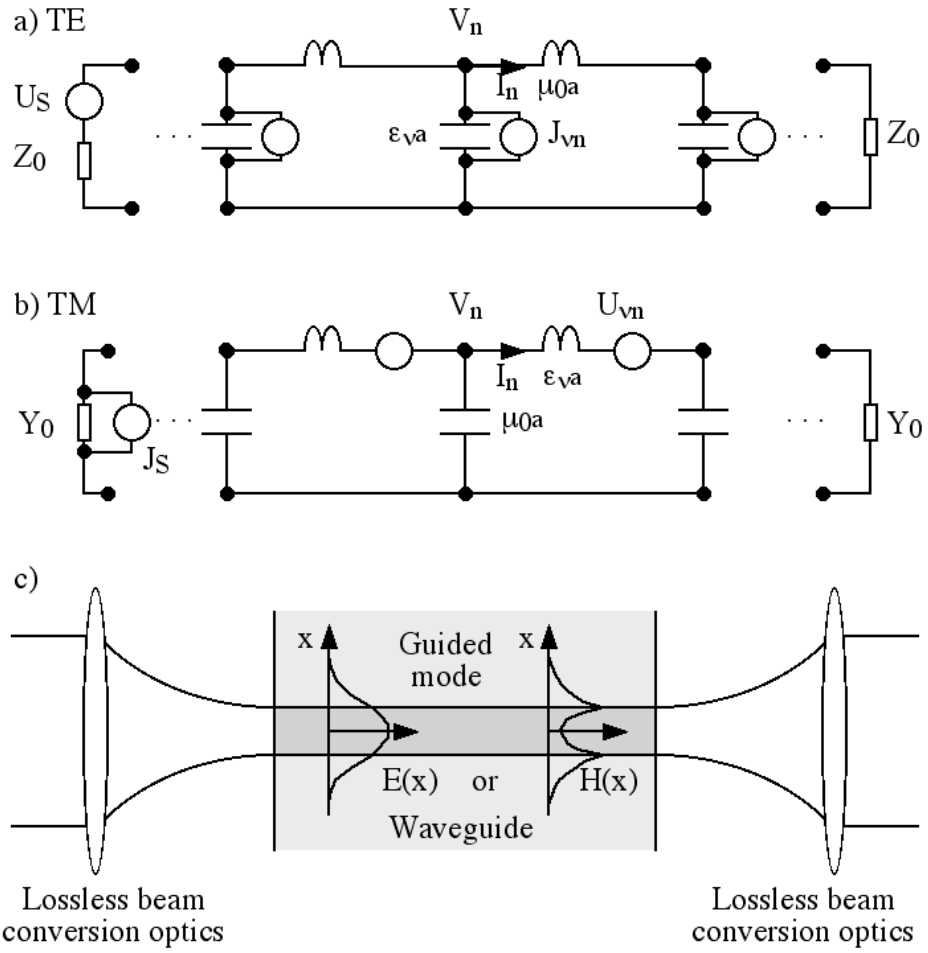

Figure 3. 1D transmission line models for a) TE and b) TM modes; c) interpretation.

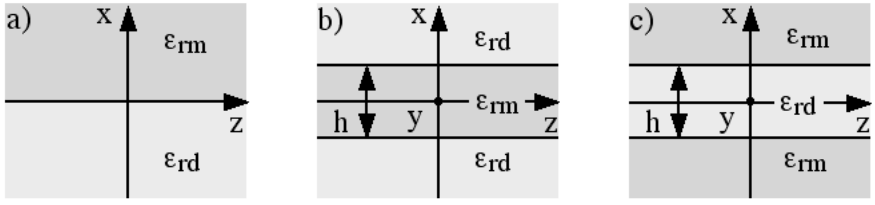

Figure 4. Geometries for a) single-interface, b) slab and c) slot plasmonic waveguides.

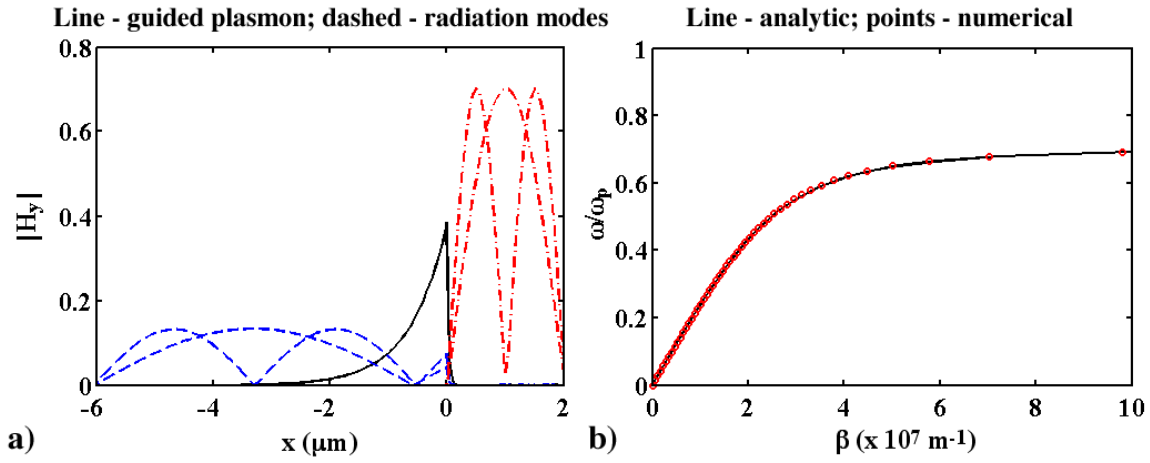

Figure 5. a) Transverse variation of $|H_y|$ for the guided mode and some low-order radiation modes supported at a single interface, as calculated using the matrix method; b) comparison between the predictions of analytic theory and the matrix method for the dispersion characteristics of a single-interface plasmon.

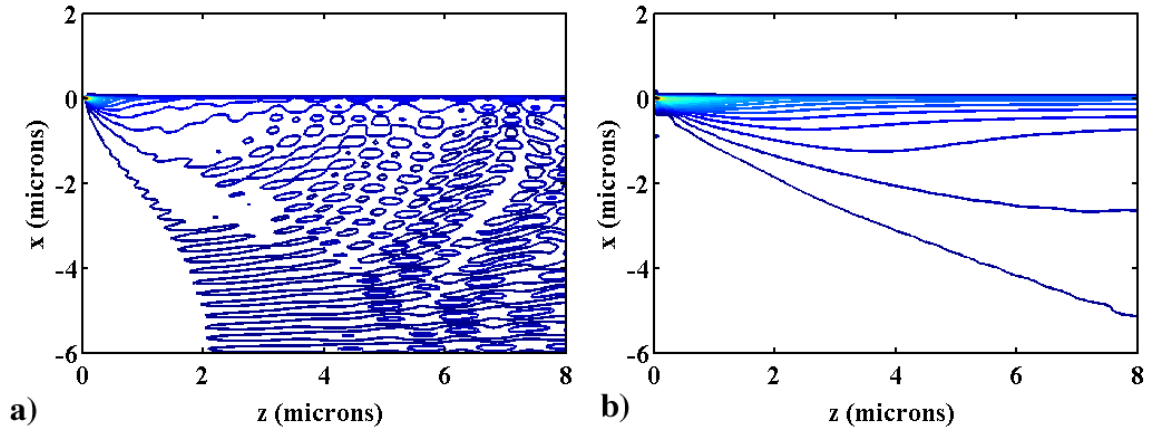

Figure 6. Two-dimensional variation of $|H_y|$ generated by the two noise sources at $(0, 0)$, calculated a) without and b) with absorbing boundaries in the matrix $\underline{A}$.

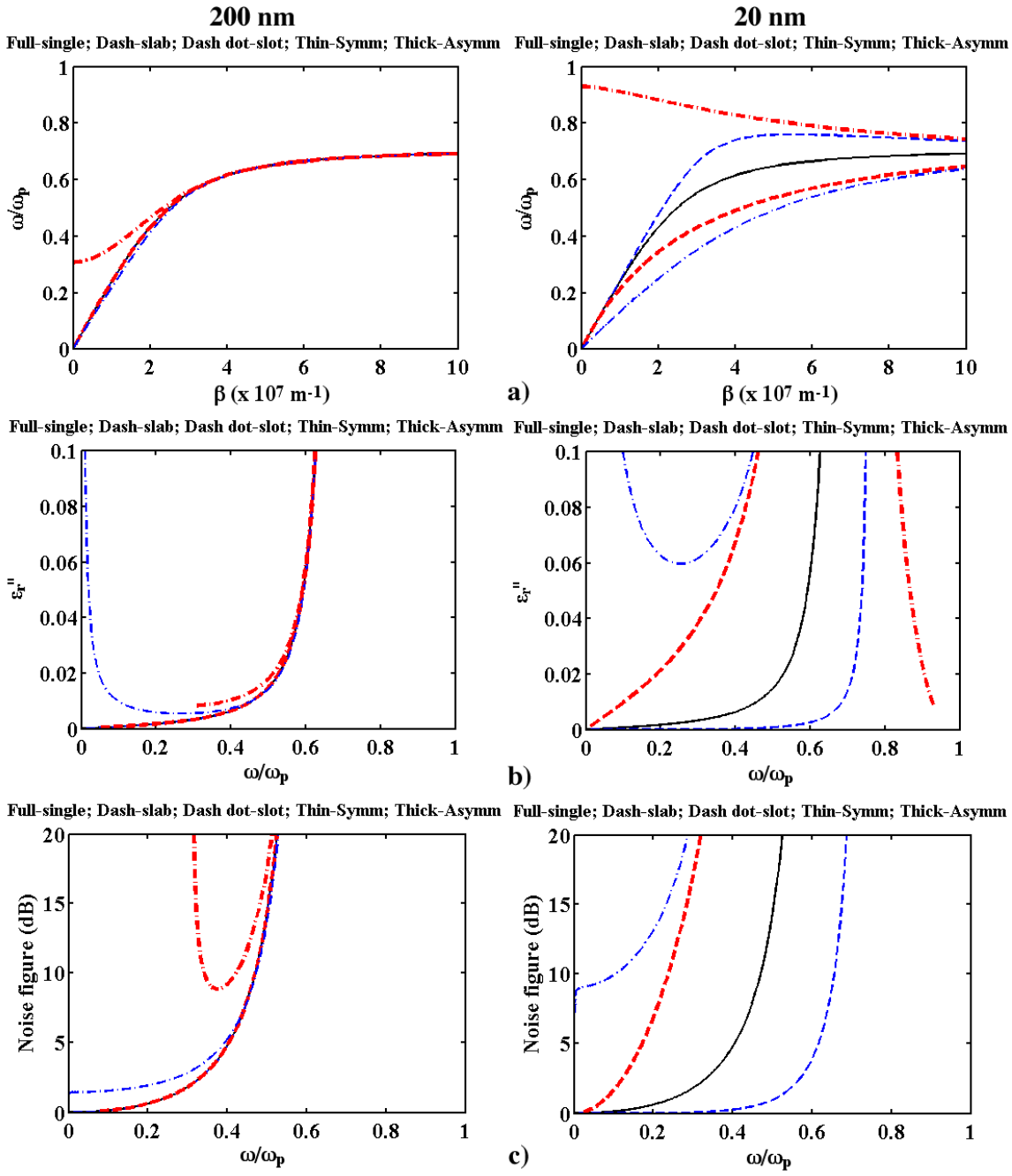

Figure 7. a) Dispersion characteristic and b) and c) frequency variation of ε_{r}'' and the noise figure for plasmons on single interfaces, slabs and slots. Two sets of data are shown: h = 200 nm (LH) and h = 20 nm (RH). The propagation distance is 10 μm.